Journal of Chromatography A 1752 (2025) 465976

Contents lists available at ScienceDirect

Journal of Chromatography A

journal homepage: www.elsevier.com/locate/chroma

Effect of stationary phase surface chemistry and particle architecture in proteomics

Jan Valášek, Lukáš Hekerle, Martina Nechvátalová, Antonín Bednařík, Jan Preisler, Jiří Urban *

Department of Chemistry, Faculty of Science, Masaryk University, Kamenice 5, 625 00 Brno, Czech Republic

ARTICLE INFO

Keywords:
Gradient elution
Column characterization
Reversed-phase retention
Bottom-up
Proteomics
Peptide

ABSTRACT

The kinetic properties of four columns packed with fully porous particles and three with superficially porous particles were characterized for possible application in proteomic bottom-up analyses. All columns provided an attachment of hydrophobic C18 chains at the surface of the stationary phase. However, they differed in the additional attachment of polar groups and/or endcapping procedure. We have used the retention modeling protocol to explore the separation efficiency and maximal achievable peak capacity on tested columns. Almost all columns provided comparable maximal peak capacity in the range of 500 – 700 for the eight-hour gradient run. This confirms that the family of the stationary phases used in the bottom-up proteomics can be extended. In the case of fully porous particles, we found that the higher the column peak capacity, the higher the number of identified peptides in the simple proteomic sample, with approximately one identified peptide per peak capacity unit. On the contrary, in the case of the superficially porous particles, the number of identified peptides in the sample decreased with the higher column peak capacity. This trend can be overturned only when the lower amount of the sample is injected. Hence, when bottom-up proteomics is considered, the lower loadability of the superficially porous particles still needs to be addressed. Most stationary phases tested can be successfully used in the bottom-up analyses. However, the stationary phases with incorporated polar functional groups reduced the undesirable contribution of free silanol groups to peptide peak tailing and increased the information provided by LC-MS analysis.

1. Introduction

In the most widespread bottom-up proteomics analysis, the proteins are first digested into particular peptides, which are then separated and identified by liquid chromatography coupled to the mass spectrometry (LC-MS) [1]. This protocol is, without any doubt, the method of choice in current attempts to explore the functions of proteins in countless different samples and living systems [2]. Although mass spectrometry instruments are experiencing steep development growth and providing comprehensive knowledge and information, liquid chromatography remains a less explored part of the protocol. To address this issue, Lenco et al. [3] provided a comprehensive overview of many attributes of reversed-phase (RP) liquid chromatography that, if properly optimized, offer full utilization of highly sophisticated MS instruments.

When focusing on the types of columns applied in the separation, their literature survey revealed that >98 % of work was performed on particulate stationary phases, with fully porous particles being almost exclusively used (96 %). Interestingly, nearly half of all analyses studied were performed on Acclaim PepMap columns (Thermo Scientific, Waltham, MA, USA) [3]. This is probably because fully porous particles are readily commercially available, optimized to provide desired separation, and easily packed into narrow capillaries, providing highly sensitive separation of peptides [4,5].

Although superficially porous particles formed by the thin stationary phase on the impervious core were introduced several decades ago [6], they are only minimally used in bottom-up proteomics [3]. Even though they provide 10 – 25 % better kinetic performance, the fully porous particles are still preferred to deal with the broad dynamic concentration range in proteomic samples [7,8].

The main advantage of superficially porous particles is that they offer similar separation as sub 2 μm particles but at a maximal pressure of 40 MPa [9]. These particles provide a better quality of column packing

* Corresponding author at. Department of Chemistry, Faculty of Science, Masaryk University, Kamenice 625 00, Brno, Czech Republic.
E-mail address: urban@chemi.muni.cz (J. Urban).

https://doi.org/10.1016/j.chroma.2025.465976
Received 7 February 2025; Received in revised form 18 April 2025; Accepted 19 April 2025
Available online 20 April 2025

when compared to the columns packed with fully porous particles [10, 11]. The reduced accessible volume for analyte diffusion due to the presence of the impervious core can be advantageous for separating peptides but is essential for analyzing large proteins [12,13]. Although the lower sample loadability was attributed to the superficially porous particles, small differences in the loading behavior of superficially and fully porous particles have been shown [14,15]. This might be attributed to the fact that the layer of the superficial stationary phase still occupies a significant volume of the total particle volume. For example, the 0.23 μm thick porous layer at a spherical particle with a diameter of 1.7 μm occupies over 60 % of its total volume [3]. Nevertheless, due to their seldom use in bottom-up proteomics, the information on the peptide concentration effect on the separation properties is rather limited.

The surface area of stationary phases used in bottom-up proteomics ranges between 100 and 400 m^2/g, with corresponding pore sizes of 100 – 130 Å. It is not recommended to use particles with pore sizes smaller than 100 Å, especially if separating larger peptides is necessary [3]. Silica-based particles with C18 alkyl chains are almost exclusively used in the RP separation of peptides, while protein separations are usually performed by columns packed with C4-modified silica particles [3,16]. However, not all Si-OH functional groups are modified by hydrophobic alkyl chains. The residual silanol groups dissociate in the presence of the mobile phase and provide ionic interactions with protonated peptides. These secondary interactions with the slow kinetics then result in peak broadening. One of the most recent strategies for suppressing unwanted silanol activity is attaching positive charges at the particle surface. For this purpose, end-capping of residual silanols by polar functionalities or embedding polar groups directly to bonded ligand was developed [17, 18]. Still, although introduced more than two decades ago [19], these particles are rarely used for proteomic analysis [3].

In this work, we aim to test the effect of surface chemistry and particle architecture of reversed-phase columns on the separation quality in bottom-up proteomics analysis. We used a retention modeling approach to compare the kinetic properties of four columns with fully porous particles and three with superficially porous particles. We studied the effect of gradient time on achievable peak capacity, which is the main separation efficiency criterion in gradient elution. To show the practical applicability of tested columns in proteomics analysis, we studied the effect of column peak capacity on the maximal number of identified peptides for both the simple proteomic sample and the highly complex cell-line digest sample.

2. Experimental part

2.1. Chemicals

Trifluoroacetic acid (TFA), formic acid (FA), dithiothreitol (DTT), iodacetamide (IAA), urea, ammonium bicarbonate, trypsin from bovine pancreas, glycyl-l-phenylalanine (Gly-Phe, M_r = 222.24), l-phenylalanyl-l-phenylalanine (Phe-Phe, M_r = 312.36), [D-Trp6]-luteinizing hormone-releasing hormone (Lut, M_r = 1311.45), angiotensin II (Ang II, M_r = 1046.18), substance P (Sub P, M_r = 1347.63), renin (Renin, M_r = 1759.01), insulin chain B oxidized (Insulin, M_r = 3495.89) were purchased from Merck (St. Louis, MO, USA). Acetonitrile for gradient HPLC, acetonitrile LC/MS grade (Merck, St. Louis, MO, USA), and redistilled deionized water were used to prepare samples and the mobile phase. Proteins α-casein and β-casein from bovine milk, catalase from bovine livers, myoglobin from equine skeletal muscle, thyroglobulin from bovine thyroid, ovalbumin and bovine serum albumin (Merck, St. Louis, MO, USA) were used to prepare simple tryptic digest sample. Pierce HeLa Protein Digest Standard was purchased from Thermo Fischer Scientific (Waltham, MA, USA)

2.2. Sample preparation

Model peptide mixture. Gly-Phe, Phe-Phe, Lut, and Ang II stock solutions were prepared in 400 μg/mL concentrations. Sub P and Insulin solutions were prepared in 200 μg/mL concentrations. A stock solution of renin was prepared at 100 μg/mL. Peptides were dissolved in 1 % Acetonitrile + 0.1 % TFA (all v/v). The final sample was prepared by mixing the stock solutions to the resulting peptide concentrations of 20 μg/mL Gly-Phe, Phe-Phe, Lut, An II, 30 μg/mL of Sub P and renin, and 50 μg/mL of insulin. The injected sample volume was 5 μL.

Tryptic digest of proteins. Stock protein solutions were prepared at 10 mg/mL concentrations in 8 M urea and 50 mM ammonium bicarbonate buffer [20]. The stock solutions were then mixed in equal proportions to give a final mixture with a concentration of 10 mg of protein per ml of solution. From this mixture, 5 mL was taken, to which 125 μL of 2 M DTT was added to disrupt the disulfide bridges. The sample was tempered in a water bath at 37 °C for one hour. Subsequently, 1 mL of 0.5 M IAA was added to alkylate the sulfide residues, and the sample was left for 30 min at laboratory temperature in the dark. Then 125 μL of 2 M DTT was added to prevent excessive alkylation, and the sample was left in the dark at laboratory temperature for additional 30 min. An aliquot of the 1 ml sample was diluted five times with 50 mM ammonium bicarbonate and then subjected to enzymatic cleavage, which was achieved by adding 100 μL of 1 mg/mL trypsin solution. The sample was incubated in a water bath at 37 °C for 24 h. Proteolytic cleavage was subsequently terminated by adding 50 μL of FA. The sample was stored at −20 °C. Before analysis, the sample was diluted 100 times with 50 mM ammonium bicarbonate buffer. The injected sample volume was 25 μL, corresponding to approximately 4 μg of digested proteins. When the effect of sample concentration on the kinetic properties of superficially porous particles was studied, 5 μL of the diluted sample was injected, providing 800, 400, and 200 ng of peptides originating from the protein sample.

HeLa Protein Digest Standard. The HeLa peptide sample was prepared by dissolving 20 μg Pierce HeLa Protein Digest Standard in 100 μL 0.1 % FA (v/v). The injected sample volume was 20 μL, corresponding to 4 μg of peptides.

2.3. Columns and instrumentation

The following columns were included in the study: Acquity UHPLC BEH C18 1.7 μm (Waters, Milford, MA, USA), Arion Plus C18 UHPLC column 1.7 μm (Chromservis, Prague, Czech Republic), Kinetex EVO C18, 1.7 μm; Kinetex Polar C18, 2.6 μm; Kinetex XB-C18, 1.7 μm; Luna Omega Polar C18, 1.6 μm; Luna Omega PS C18, 1.6 μm (all Phenomenex, Torrance, CA, USA). The dimensions of all columns tested were 150 × 2.1 mm (L x ID). Table 1 summarizes the surface chemistry and hydrodynamic properties of characterized columns with fully and superficially porous particles.

All experiments were performed on an UltiMate 3000 RS System (ThermoFisher, Waltham, MA, USA) equipped with a binary high-pressure pump, autosampler, temperature-controlled column compartment, and variable wavelength detector set at 214 nm. The experimental gradient delay volume of the ThermoFisher UltiMate 3000 RS system (V_D = 0.164 mL) was determined as suggested by Lenco [3]. The experimental method in software has not compensated for the gradient delay volume.

For the LC-MS/MS analysis, the UltiMate 3000 RS System was combined with a Q Exactive Plus mass spectrometer (ThermoFisher, Waltham, MA, USA) using the original IonMax ionization source and HESI II probe. Capillary temperature was held at 250 °C. The spray voltage was 4.1 kV, and the S-lens radio frequency level was 50. The gas flow rate values for sheath, auxiliary, and sweep gas were 25, 6, and 0, respectively. Signals were acquired in positive mode. The top 10 precursors were selected for data-dependent acquisition (DDA) of MS/MS spectra. For full MS, mass resolution was 70,000, Automatic Gain Control (AGC) target $5 \cdot 10^{6,}$ and maximum injection time 50 ms. The detection range was 350 to 2000 *m/z*. For MS/MS, mass resolution was 17,500, AGC target $5 \cdot 10^{4,}$ and maximum injection time 145 ms. Nominal collision energy value was 30.

Table 1
The surface chemistry and hydrodynamic properties of characterized columns.
Name – Characterized columns. See Section 2.3 for brand names and manufacturers of the columns. d_p, μm – particle size. ε_T – column total porosity determined by elution volume of uracil in 1 % acetonitrile + 0.1 % formic acid at 40 °C (Eq. (2)). K_F, m^2 – column permeability calculated by Eq. (1). Pore size, Å – pores size. Carbon load, % - carbon load in the stationary phase. Surface area, m^2/g – the surface area of the stationary phase. Layer thickness, μm – thickness of the porous layer on superficially porous particles. The dimensions of all columns tested were 150 × 2.1 mm (L x ID). n.a. – not available.

Column	Name	d_p, μm	ε_T	K_F, m^2	Pore size, Å	Carbon load, %	Surface area, m^2/g	Layer thickness, μm
1	Acquity	1.7	0.73	$1.95 \cdot 10^{-15}$	130	18	185	–
2	Arion	1.7	0.73	$1.70 \cdot 10^{-15}$	100	n.a.	420	–
3	Kinetex Evo	1.7	0.59	$2.28 \cdot 10^{-15}$	100	11	200	0.23
4	Kinetex Polar	2.6	0.63	$2.89 \cdot 10^{-15}$	100	9	200	0.23
5	Kinetex XB	1.7	0.63	$2.22 \cdot 10^{-15}$	100	10	200	0.23
6	Luna Polar	1.6	0.72	$2.00 \cdot 10^{-15}$	100	11	260	–
7	Luna PS	1.6	0.73	$1.98 \cdot 10^{-15}$	100	11	260	–

MaxQuant 2.6.6.0 software [21] analyzed the raw LC-MS files with carbamidomethyl fixed modification and oxidation and acetylation as variable modifications. Trypsin/P was selected as the digestion enzyme. FASTA files for individual proteins and human proteome were downloaded from the UniProt database (https://www.uniprot.org/). The number of peptides determined in each raw file was extracted from the *Evidence table* after removing peptides marked as Potential contaminants.

2.4. Columns characterization & calculations

The column permeability, K_F (Eq. (1)), and total porosity, ε_T (Eq. (2)), characterized the hydrodynamic properties of tested columns.

$$K_F = \frac{F \cdot \eta \cdot L}{\Delta p \cdot \pi \cdot r^2} \tag{1}$$

$$\varepsilon_T = \frac{V_0}{V_C} \tag{2}$$

In Eqs. (1) and (2), F is the mobile-phase flow rate (m^3/s), η is the mobile-phase viscosity (Pa·s), Δp is the pressure drop across the column (Pa), L is the column length (m), r is the column inner radius (m), V_0 is the column hold-up volume (mL), and V_C is a geometrical volume of the empty cylindrical column (mL).

To explore the retention behavior of peptides on tested columns, we have used a retention modeling approach utilizing the linear solvent strength theory introduced by Snyder [22] and extended to a general form by Jandera [23]. Retention times, t_R, and baseline peak widths, w, of seven peptides were determined in several scouting runs differing in the gradient slope, B_g, characterizing the linear increase in the initial acetonitrile concentration, φ_0, to final concentration, φ_F, in the frame of preselected gradient time, t_G, as shows Eq. (3).

$$B_g = \frac{\varphi_F - \varphi_0}{t_G} \tag{3}$$

The gradient times were varied to provide gradient slopes, B_g, in the 0.008 – 0.049 min^{-1} range. However, to ensure that all analytes undergo a similar gradient history during the elution [24], we varied the mobile phase flow rate to keep the volumetric gradient slope constant at 0.08 mL^{-1}.

The experimental retention times, together with the initial gradient concentration, φ_0, gradient slope, B_g, column hold-up time, t_0, and instrument dwell time, t_D, were fitted to Eq. (4) to extract the retention characteristics of individual peptides, i.e., parameters a and S. While the parameter a is the logarithm of retention factor of analyte in the fully aqueous mobile phase, the parameter S depends on the analyte size and type of the mobile and stationary phase [25]. Knowledge of these parameters then allows us to predict the retention behavior of tested peptides in any gradient profile [23]:

$$t_R = \frac{1}{S \cdot B_g} \log\left[2.3 \cdot S \cdot B_g \cdot \left(t_0 \cdot 10^{(a - S \cdot \varphi_0)} - t_D\right) + 1\right] + t_0 + t_D \tag{4}$$

The important parameter in column characterization is its separation efficiency, which is described by the number of theoretical plates, N, calculated from the retention time of the analyte, t_R, and baseline peak width, w, by equation Eq. (5), where L is the column length (m) and $HETP$ is the height equivalent to a theoretical plate (m).

$$N = 16 \cdot \left(\frac{t_R}{w}\right)^2 = \frac{L}{HETP} \tag{5}$$

To calculate the number of theoretical plates in the gradient elution, N_g (Eq. (6)), we utilized experimental baseline peak widths, w, and retention factor at the time of elution from the column, k_e (Eq. (7)), of Substance P ($M_r = 1348$) as a peptide with the average molecular mass within the tested peptides.

$$N_g = 16 \cdot \left[\frac{t_0 \cdot (1 + k_e)}{w}\right]^2 \tag{6}$$

$$k_e = \frac{1}{2.3 \cdot S \cdot B_g \cdot t_0 + 10^{(S \cdot \varphi_0 - a)}} \tag{7}$$

To confirm the validity of this approach, we then used the number of theoretical plates determined for Substance P to calculate theoretical baseline peak widths (Eq. (8)) of tested peptides in scouting gradients used.

$$w = \frac{4 \cdot t_0}{\sqrt{N_g}} (1 + k_e) \tag{8}$$

In the next step, we explored the effect of the linear velocity of the mobile phase, u (mm/s), on separation efficiency expressed as height equivalent to a theoretical plate, $HETP$ (μm), which is described by van Deemter equation (Eq. (9)) [26].

$$HETP = 2\lambda d_p + 2X\frac{D_m}{u} + c\frac{d_p^2}{D_m}u \tag{9}$$

In Eq. (9), λ is the packed bed structural uniformity factor, X is the obstruction factor, c is related to mass transfer resistance, and D_m is the Substance P diffusion coefficient calculated from the Young equation [27]. Volumetric flow rates of the mobile phase, F, were transformed to the linear velocity of the mobile phase by Eq. (10), where ε_T is the total porosity of the column, and r is the column radius.

$$u = \frac{F}{\varepsilon_T \pi r^2} \tag{10}$$

Although there are several different protocols for determining peak capacity in liquid chromatography [28,29], one of the most straightforward approaches is the calculation of "sample peak capacity", introduced by Snyder [30], considering only a fraction of the separation window is utilized by the sample. Sample peak capacity was calculated by Eq. (11), where $t_{R,1}$ and $t_{R,n}$ are retention times of the first and the last eluted peak, respectively, and w_{avr} is the average peak baseline width within the gradient run. Sample peak capacity is used throughout this manuscript to characterize the separation quality on tested columns.

$$n_c = \frac{t_{R,n} - t_{R,1}}{w_{avr}} \quad (11)$$

As the achievable peak capacity depends on several experimental variables, such as gradient time, mobile phase flow rate, column temperature, and final acetonitrile concentration [31], optimizing these variables for each gradient time is also necessary. For that, we have adopted a graphical method of peak capacity optimization introduced by Wang et al. [32], where for a fixed gradient time, t_G, the mobile phase flow rate, F, and final acetonitrile gradient concentration, φ_F, were simultaneously varied to maximize the calculated peak capacity, n_c. The calculated peak capacity is then plotted versus the gradient time to construct the final kinetic plot [33].

3. Results and discussion

3.1. Hydrodynamic properties of the columns

In this work, we studied the effect of surface chemistry and particle architecture on the kinetic properties of four fully porous and three superficially porous reversed-phase particles, focusing on the separation quality in bottom-up proteomics.

Table 1 lists the basic properties of characterized columns. All columns tested possess the C18 functionality attached to the stationary phase, while they differ in the additional surface modification. The hydrophobic chains at the Arion stationary phase are endcapped in a multistep reaction. Trifunctionally bonded ethylene bridged hybrid (BEH) particles of the Acquity column improve the pH stability of the column. In contrast, di-isobutyl side chains in the Kinetex XB stationary phase improve peak shape and increase retention of acidic compounds. An organo-silica grafting process incorporates stabilizing ethane cross-linking to the surface of the Kinetex EVO column, providing resistance to high pH. The polar functional groups modify the surface of the Kinetex Polar and Luna Polar stationary phases, providing enhanced polar retention and aqueous stability. The Luna PS column contains a positive charge, helping retain acidic compounds and providing a better peak shape for bases through ionic interactions.

Unsurprisingly, columns packed with fully porous particles provided higher values of column total porosity, ε_T (Table 1). The porosity of superficially porous particles is smaller by approximately 10 %, corresponding to the impervious core volume inside these particles. The reduction in the total pore volume also reflects the values of columns' permeability, which is higher for columns packed with superficially porous particles. Almost all columns provided a pore size of 100 Å (the pore size of the Acquity column is 130 Å), which is in the ideal range suitable for the analysis of peptides [3,34]. Indeed, the hydrodynamic size of the largest peptide from the model mixture (Insulin B oxidized chain, $M_r = 3496$) is 30.7 Å [34], suggesting that no steric limitations occur during the analysis on tested columns.

Overall, all columns provided similar hydrodynamic properties differing only based on the architecture of the particles.

3.2. Retention modeling

Table SI-1 summarizes the extracted values of retention parameters for the peptide model mixture on the characterized columns at 40, 50, and 60 °C column temperatures. High values of correlation coefficients, R, and low values of overall root mean square error (RMSE) confirm the validity of the linear solvent strength model in the retention behavior description of peptides on all reversed-phase columns. Both parameters, a and S, increase with the size of the analyte, slightly decrease with higher column temperature, and, to some extent, vary between individual columns.

The parameter S is the slope of the function logarithm of the retention factor, k, versus the volume fraction of the acetonitrile in the mobile phase, φ [23,35]. These linear curves are usually shallow for the small molecules, and the S parameter values can be determined from isocratic data. However, in the case of larger analytes, such as peptides or proteins, the possibilities of isocratic elution are minimal, as the practically useful range of acetonitrile concentrations is too narrow. Hence, for peptides, parameter S can be either extracted from gradient scouting runs (**Table SI-1**), calculated based on some theoretical assumptions [3, 26], or predicted from the sequence of the peptides [36].

We compared parameter S determined from experimental data to those predicted by Gilar [26]. In Eq. (12), the M_r is the molecular mass of the peptide, and literature data are $p = 0.6915$ and $q = 1.49$.

$$\ln S = p \cdot \ln M_r - q \quad (12)$$

Determined values of intercepts and slopes of Eq. (12) for tested columns agree well with those suggested by Gilar, as demonstrated in **Table SI-2**. The values of parameter S calculated for a hypothetical peptide with $M = 2000$ are 25.3 to 33.0, with most columns closer to the higher value. These results correspond well with the assumption that peptide parameter S values are between 29 and 38 [3,36,37]. There is no significant effect of particle architecture on the values of parameter S. This might be, at least partially, explained by the fact that parameter S is related mainly to the molecular mass of the analyte. Also, the differences in the stabilization of the C18 alkyl chains at the surface of the particles from different manufacturers are not reflected in the values of parameter S, as all experimental characterization involved a reversed-phase retention mechanism with an aqueous acetonitrile mobile phase and hydrophobic surface with C18 alkyl chains.

It should be pointed out that we also tested the effect of temperature on the parameters p and q in Eq. (12). However, the impact of molecular mass on parameter S was significantly smaller on all columns at elevated temperatures, leading to the lower values of slopes p with an average value of $p = 0.028$ and 0.069 at 50 and 60 °C, respectively. As column temperature seems to be one of the overlooked optimization parameters in proteomic separations [37], we plan to explore the low sensitivity of parameter S on analyte molecular mass at higher column temperatures in our laboratory further in the future.

3.3. Separation efficiency

Unlike in isocratic elution, where separation efficiency is determined directly from the retention data (Eq. (5)), this is impossible in gradient elution. Several protocols, including the application of the plate number determined under isocratic conditions in mobile phases of analyte elution or "median" plate number, are usually utilized in the first approximation [35]. Recently, we confirmed that gradient elution data can be used to obtain separation efficiency. The van Deemter curves constructed from gradient data agreed well with those determined in the isocratic mobile phase [33]. Hence, in this work, we used the gradient elution data to construct van Deemter curves and compare the separation efficiency of the tested columns.

Table SI-3 compares the experimental and calculated average baseline peptide peak widths (Eq. (8)) of all gradients at individual columns. The calculated average baseline peak widths agree well with those experimental ones, further confirmed by high values of correlation coefficients and low values of root mean square errors.

In the next step, the values of height equivalent to the theoretical plate, *HETP*, calculated for Substance P from the gradient column efficiencies, N_g, determined at three to four mobile phase linear velocities, u, were fitted by Eq. (9). **Table SI-4** summarizes the best-fit parameters (λ, X, c), regression coefficients and root mean square error values. In most cases, the packed bed structural uniformity factor, λ, showed minimal values, suggesting that all tested columns were packed well and had minimal packing irregularities. With two exceptions (Kinetex XB at 40 °C and Arion at 50 °C), the obstruction factor X shows higher values for superficially porous particles when compared to columns packed with fully porous particles. The reason might be that the pore size distribution of superficially porous particles is narrower when compared to

that of fully porous particles. Surprisingly, parameter *c*, which is related to the mass transfer resistance factor, increased with the higher values of column temperature. The highest contribution to mass transfer resistance showed columns Arion and Luna PS, with the lowest values of parameter *c* showing the column Kinetex Polar, followed by column Kinetex XB and Acquity. Although particle architecture generally has no significant effect, superficially porous particles provide slightly lower mass transfer resistance parameter values, especially at lower column temperatures.

Fig. 1 compares the effect of mobile phase linear velocity on the separation efficiency (expressed as *HETP*, μm) at three different column temperatures. The most efficient columns are Acquity and Luna Polar, followed by columns with superficially porous particles (Kinetex XB, Kinetex Polar, and Kinetex EVO). The least efficient columns are Luna PS and Arion (except for 60 °C, where Arion switched the place with the Kinetex Polar column).

3.4. Peak capacity optimization

Peak capacity is the main criterion describing the separation quality in gradient elution chromatography. It represents the theoretical number of peaks that fit the separation space with a resolution $R = 1$ [24,38,39].

The sample peak capacity calculated for optimal mobile phase flow rate, and the final acetonitrile concentration was plotted against various gradient times to construct kinetic plots (Section 2.4) [32]. Fig. 2 describes the effect of gradient time on achievable peak capacity for individual columns at column temperatures of (A) 40 °C, (B) 50 °C, and (C) 60 °C. As expected, the achievable peak capacity is higher at higher column temperatures.

In terms of gradient elution separation efficiency, expressed by the achievable sample peak capacity, the most efficient are column Luna Polar (at 40 and 50 °C) and columns Luna PS and Acquity (at 60 °C). On the other hand, Arion and Kinetex Polar columns provided the lowest gradient elution separation efficiency at all column temperatures. However, it should have been pointed out that, in general, most columns tested provided comparable values of maximal sample peak capacity, varying 5 – 10 % when compared to the maximal calculated value. The exceptions are columns Kinetex Polar and Arion, which provide 15 and 25 % lower maximal peak capacity, respectively (compared to the maximal value at a particular column temperature).

3.5. Analysis of proteomic samples

So far, the columns were characterized by maximal peak capacity determined by the retention modeling approach. In the next step, we explored the effect of column hydrodynamic properties (Table 1) on the number of peptides identified within a one-hour gradient running at 50 °C. The number of peptides identified in the simple proteomic sample correlates well with the column permeability. The higher the permeability, the more peptides were identified, as demonstrated in **Figure SI-1**. This result suggests that permeability might be another column parameter allowing optimization of the information the proteomic analysis provides.

To explore the practical utilization of tested columns in proteomics analyses, we have compared the peak capacity calculated for a one-hour gradient running at 50 °C with the number of peptides determined at the same experimental conditions for the tryptic digest of seven proteins.

Fig. 3 shows the correlation between the number of identified peptides and the calculated peak capacity. As expected, the number of identified peptides increases for columns with higher peak capacity. However, a closer examination reveals that this observation is valid only for columns with fully porous particles. At the same time, there is a decrease in the number of extracted peptides with higher peak capacity for columns packed with superficially porous particles.

The results presented in Fig. 3 propose a negative link between the number of determined peptides and achievable peak capacity for columns with superficially porous particles. Hence, we have tested the effect of sample load on three columns with superficially porous particles (Fig. 4). With the decrease in the injected amount of peptides from 4 μg (circles) to 0.8 μg (triangles), 0.4 μg (stars), and 0.2 μg (hexagons), respectively, the negative trend between the number of identified peptides and determined peak capacity became flatter confirming the strong effect of analyte concentration on the kinetic properties of superficially porous particles. Although it has been shown that the loadability of superficially porous particles is comparable with that of fully porous particles when small molecules are used as the characterization markers [14,15], our results suggest that this is not the case for peptides, and a decrease in the analyte concentration is necessary to fully utilize the separation potential of columns packed with superficially porous particles. On the other hand, results derived from Fig. 4 suggest that the superficially porous particles might find their application in the case of low amounts of injected proteomic samples, such as single-cell analysis [40].

Finally, to further test the applicability of the tested columns in proteomics, we have selected four columns combining the highest and lowest achievable peak capacity and examined their separation power in the analysis of complex HeLa cell digest samples. Fig. 5 compares a number of identified peptides to the achievable peak capacity for an optimized one-hour gradient run at a column temperature of 50 °C. Again, the columns with higher separation efficiency (i.e., peak capacity) described the sample better. On the other hand, regarding the number of determined peptides, the difference between one column with superficially porous particles and two Luna columns with fully porous particles is minimal, suggesting that all of them can be successfully applied in proteomics analyses.

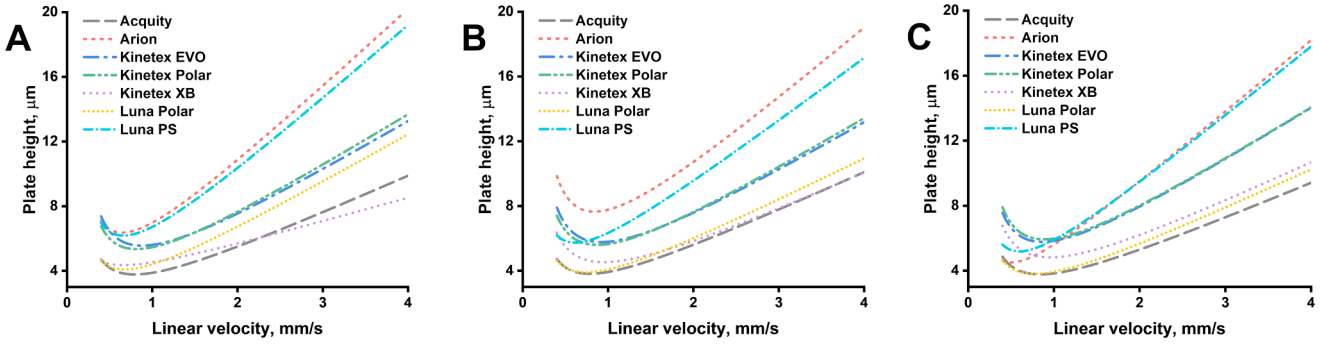

Fig. 1. Van Deemter curves calculated from gradient elution data for Substance P at (A) 40, (B) 50, and (C) 60 °C. Plate height, μm – height equivalent to theoretical plate; Linear velocity, mm/s – mobile phase linear velocity. Columns as in Table 1.

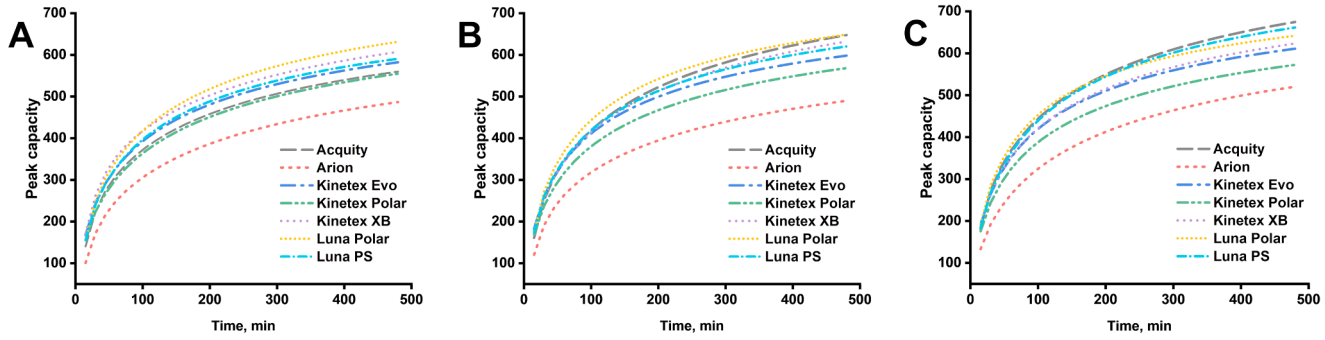

Fig. 2. Kinetic plots for tested columns determined at (A) 40, (B) 50, and (C) 60 °C. Peak capacity – peak capacity calculated for a particular gradient time by Eq. (11). Time, min – predefined gradient time. See Section 2.4 for information on kinetic plot characterization. Columns as in Table 1.

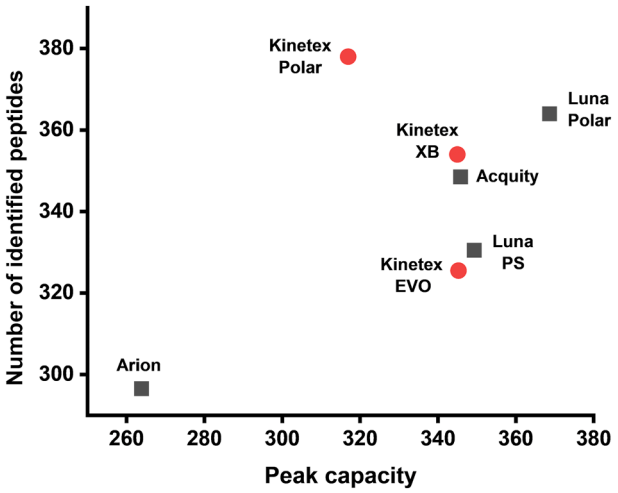

Fig. 3. Effect of column peak capacity on the number of peptides identified in a tryptic digest of seven proteins. Peak capacity – peak capacity of individual columns calculated by Eq. (11) for gradient time 1 h at a column temperature of 50 °C. Number of identified peptides – the number of peptides determined in the sample during the experimental gradient running for 1 h at a column temperature of 50 °C. Squares – columns with fully porous particles. Circles – columns with superficially porous particles. The amount of injected peptides 4 μg. Columns as in Table 1.

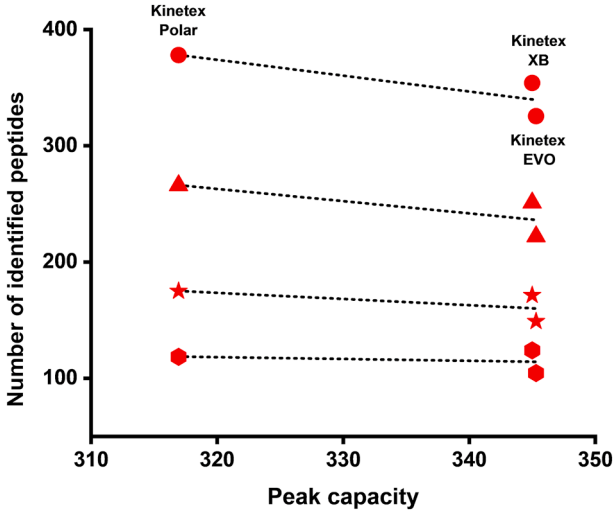

Fig. 4. Effect of sample loading on column peak capacity of columns with superficially porous particles and the number of peptides identified in a tryptic digest of seven proteins. Peak capacity – peak capacity of individual columns calculated by Eq. (11) for gradient time 1 h at a column temperature of 50 °C. Number of identified peptides – the number of peptides determined in the sample during the experimental gradient running for 1 h at a column temperature of 50 °C. Circles – the amount of injected peptides 4 μg. Triangles – the amount of injected peptides 0.8 μg. Stars – the amount of injected peptides 0.4 μg. Hexagons – the amount of injected peptides 0.2 μg. Columns as in Table 1. Trendlines are added to guide eyes.

4. Conclusions

In this work, we explored the effect of particle architecture and stationary phase surface chemistry on the quality of the separation in bottom-up proteomics. Four columns with fully porous particles and three with superficially porous particles were compared. The retention modeling approach was successfully applied to characterize the columns' kinetic properties. All columns tested provided agreement between their retention behavior and the gradient elution reversed-phase liquid chromatography theory. The separation efficiency of gradient elution, expressed as the sample peak capacity, improved with the column temperature. The higher achievable peak capacity columns provided more peptides identified within the simple protein digest sample. However, for columns packed with superficially porous particles, these findings were valid only at the reduced amount of the injected sample, suggesting that sample concentration still plays a significant role in their chromatographic behavior. We have also compared the provided peak capacity to a number of identified peptides in complex cell line digest. Again, the number of identified peptides increased with higher gradient separation efficiency, although the overall differences were not so dramatic. Although the variations in the kinetic properties for most tested columns were minimal, the columns possessing the polar groups at their surface performed better.

The presented results suggest that broadening the family of stationary phases used in bottom-up proteomics is advantageous. Although the differences between stationary phases might seem subtle, properly selected particle architecture and surface chemistry improve the quality of information provided by particular proteomic applications. While the superficially porous particles might find their application in low-input proteomic analyses, incorporating polar groups into the surface of the stationary phases reduces the undesirable contribution of free silanol

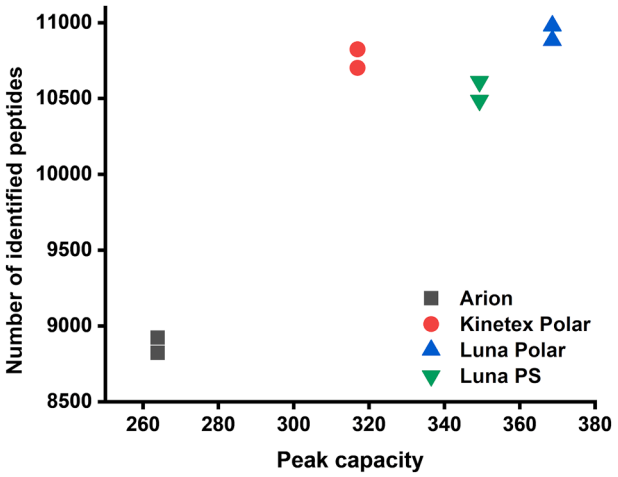

Fig. 5. Effect of column peak capacity on the number of peptides identified in HeLa cell line tryptic digest technical replicates. Peak capacity – peak capacity of individual columns calculated by Eq. (11) for gradient time 1 h at a column temperature of 50 °C. Number of identified peptides – the number of peptides determined in the sample during the experimental gradient running for 1 h at a column temperature of 50 °C. Columns as in Table 1.

groups to peptide peak tailing and considerably increases the information provided by LC-MS analysis.

CRediT authorship contribution statement

Jan Valášek: Methodology, Investigation, Data curation. **Lukáš Hekerle:** Methodology, Investigation, Data curation. **Martina Nechvátalová:** Methodology, Investigation. **Antonín Bednařík:** Writing – review & editing, Methodology. **Jan Preisler:** Writing – review & editing. **Jiří Urban:** Conceptualization, Writing – original draft, Writing – review & editing, Supervision, Funding acquisition.

Declaration of competing interest

The authors declare that they have no known competing financial interests or personal relationships that could have appeared to influence the work reported in this paper.

Acknowledgment

The financial support of the Czech Science Foundation project 23–07581S is gratefully acknowledged.

Supplementary materials

Supplementary material associated with this article can be found, in the online version, at doi:10.1016/j.chroma.2025.465976.

Data availability

Data will be made available on request.

References

[1] Y. Zhang, B.R. Fonslow, B. Shan, M.-C. Baek, J.R. Yates, Protein analysis by shotgun/bottom-up proteomics, Chem. Rev. 113 (2013) 2343–2394, https://doi.org/10.1021/cr3003533.
[2] T.M. Peters-Clarke, J.J. Coon, N.M. Riley, Instrumentation at the leading edge of proteomics, Anal. Chem. 96 (2024) 7976–8010, https://doi.org/10.1021/acs.analchem.3c04497.
[3] J. Lenco, S. Jadeja, D.K. Naplekov, O. Krokhin, M.A. Khalikova, P. Chocholous, J. Urban, K. Broeckhoven, L. Novakova, F. Svec, Reversed-phase liquid chromatography of peptides for bottom-up proteomics: a tutorial, J. Proteome Res. 21 (2022) 2846–2892, https://doi.org/10.1021/acs.jproteome.2c00407.
[4] D. Bell, Evolutions in particle, surface chemistry, and hardware designs: new liquid chromatography (LC) columns and accessories for 2024, 1 (2024) 14–22.
[5] K. Broeckhoven, G. Desmet, Advances and innovations in liquid chromatography stationary phase supports, Anal. Chem. 93 (2021) 257–272, https://doi.org/10.1021/acs.analchem.0c04466.
[6] C.G. Horvath, S.R. Lipsky, Rapid analysis of ribonucleosides and bases at the picomole level using pellicular cation exchange resin in narrow bore columns, Anal. Chem. 41 (1969) 1227–1234, https://doi.org/10.1021/ac60279a024.
[7] M. Dams, J.L. Dores-Sousa, R.-J. Lamers, A. Treumann, S. Eeltink, High-resolution nano-liquid chromatography with tandem mass spectrometric detection for the bottom-up analysis of complex proteomic samples, Chromatographia 82 (2019) 101–110, https://doi.org/10.1007/s10337-018-3647-5.
[8] L. Tolley, J.W. Jorgenson, M.A. Moseley, Very high pressure gradient LC/MS/MS, Anal. Chem. 73 (2001) 2985–2991, https://doi.org/10.1021/ac0010835.
[9] J.M. Cunliffe, T.D. Maloney, Fused-core particle technology as an alternative to sub-2-µm particles to achieve high separation efficiency with low backpressure, J. Sep. Sci. 30 (2007) 3104–3109, https://doi.org/10.1002/jssc.200700260.
[10] G. Guiochon, F. Gritti, Shell particles, trials, tribulations and triumphs, J. Chromatography A 1218 (2011) 1915–1938, https://doi.org/10.1016/j.chroma.2011.01.080.
[11] S. Bruns, D. Stoeckel, B.M. Smarsly, U. Tallarek, Influence of particle properties on the wall region in packed capillaries, J. Chromatography A 1268 (2012) 53–63, https://doi.org/10.1016/j.chroma.2012.10.027.
[12] B. Bobály, J.-L. Veuthey, D. Guillarme, S. Fekete, New developments and possibilities of wide-pore superficially porous particle technology applied for the liquid chromatographic analysis of therapeutic proteins, J Pharm Biomed Anal 158 (2018) 225–235, https://doi.org/10.1016/j.jpba.2018.06.006.
[13] J. Urban, P. Jandera, Z. Kučerová, M.A. van Straten, H.A. Claessens, A study of the effects of column porosity on gradient separations of proteins, J. Chromatography A 1167 (2007) 63–75, https://doi.org/10.1016/j.chroma.2007.08.027.
[14] M.M. Fallas, S.M.C. Buckenmaier, D.V. McCalley, A comparison of overload behaviour for some sub 2 µm totally porous and sub 3 µm shell particle columns with ionised solutes, J. Chromatography A 1235 (2012) 49–59, https://doi.org/10.1016/j.chroma.2012.02.027.
[15] G. Kahsay, K. Broeckhoven, E. Adams, G. Desmet, D. Cabooter, Kinetic performance comparison of fully and superficially porous particles with a particle size of 5 µm: intrinsic evaluation and application to the impurity analysis of griseofulvin, Talanta 122 (2014) 122–129, https://doi.org/10.1016/j.talanta.2014.01.050.
[16] A. Bodzon-Kulakowska, A. Bierczynska-Krzysik, T. Dylag, A. Drabik, P. Suder, M. Noga, J. Jarzebinska, J. Silberring, Methods for samples preparation in proteomic research, J. Chromatogr B Analyt Technol Biomed Life Sci 849 (2007) 1–31, https://doi.org/10.1016/j.jchromb.2006.10.040.
[17] J. Layne, Characterization and comparison of the chromatographic performance of conventional, polar-embedded, and polar-endcapped reversed-phase liquid chromatography stationary phases, J. Chromatography A 957 (2002) 149–164, https://doi.org/10.1016/S0021-9673(02)00193-0.
[18] E.M. Borges, Silica, hybrid Silica, hydride Silica and non-Silica stationary phases for liquid chromatography, J. Chromatogr Sci 53 (2015) 580–597, https://doi.org/10.1093/chromsci/bmu090.
[19] A. Méndez, E. Bosch, M. Rosés, U.D. Neue, Comparison of the acidity of residual silanol groups in several liquid chromatography columns, J. Chromatography A 986 (2003) 33–44, https://doi.org/10.1016/S0021-9673(02)01899-X.
[20] H. Zhou, M. Ye, J. Dong, E. Corradini, A. Cristobal, A.J.R. Heck, H. Zou, S. Mohammed, Robust phosphoproteome enrichment using monodisperse microsphere–based immobilized titanium (IV) ion affinity chromatography, Nat. Protoc 8 (2013) 461–480, https://doi.org/10.1038/nprot.2013.010.
[21] S. Tyanova, T. Temu, J. Cox, The MaxQuant computational platform for mass spectrometry-based shotgun proteomics, Nat. Protoc 11 (2016) 2301–2319, https://doi.org/10.1038/nprot.2016.136.
[22] L.R. Snyder, J.W. Dolan, The linear-solvent-strength model of gradient elution. Advances in Chromatography, CRC Press, 1998.
[23] P. Jandera, J. Churáček, Gradient Elution in Column Liquid Chromatography: Theory and Practice, Elsevier, 1985.
[24] T.J. Causon, K. Broeckhoven, E.F. Hilder, R.A. Shellie, G. Desmet, S. Eeltink, Kinetic performance optimisation for liquid chromatography: principles and practice, J. Sep. Sci. 34 (2011) 877–887, https://doi.org/10.1002/jssc.201000904.
[25] P. Jandera, Can the theory of gradient liquid chromatography be useful in solving practical problems? J. Chromatogr. A 1126 (2006) 195–218, https://doi.org/10.1016/j.chroma.2006.04.094.
[26] M. Gilar, A.E. Daly, M. Kele, U.D. Neue, J.C. Gebler, Implications of column peak capacity on the separation of complex peptide mixtures in single- and two-dimensional high-performance liquid chromatography, J. Chromatography A 1061 (2004) 183–192, https://doi.org/10.1016/j.chroma.2004.10.092.
[27] M. Young, P. Carroad, R. Bell, Estimation of diffusion-coefficients of proteins, Biotechnol. Bioeng. 22 (1980) 947–955, https://doi.org/10.1002/bit.260220504.
[28] U.D. Neue, Peak capacity in unidimensional chromatography, J. Chromatogr. A 1184 (2008) 107–130, https://doi.org/10.1016/j.chroma.2007.11.113.
[29] U.D. Neue, Theory of peak capacity in gradient elution, J. Chromatog.r A 1079 (2005) 153–161, https://doi.org/10.1016/j.chroma.2005.03.008.
[30] J.W. Dolan, L.R. Snyder, N.M. Djordjevic, D.W. Hill, T.J. Waeghe, Reversed-phase liquid chromatographic separation of complex samples by optimizing temperature and gradient time I. Peak capacity limitations, J. Chromatogr. A 857 (1999) 1–20, https://doi.org/10.1016/S0021-9673(99)00765-7.

[31] X. Wang, D.R. Stoll, A.P. Schellinger, P.W. Carr, Peak capacity optimization of peptide separations in reversed-phase gradient elution chromatography: fixed column format, Anal. Chem. 78 (2006) 3406–3416, https://doi.org/10.1021/ac0600149.
[32] X. Wang, D.R. Stoll, P.W. Carr, P.J. Schoenmakers, A graphical method for understanding the kinetics of peak capacity production in gradient elution liquid chromatography, J. Chromatogr. A 1125 (2006) 177–181, https://doi.org/10.1016/j.chroma.2006.05.048.
[33] A. Kosmakova, Z. Zajickova, J. Urban, Characterization of hybrid organo-silica monoliths for possible application in the gradient elution of peptides, J. Sep. Sci. 46 (2023), https://doi.org/10.1002/jssc.202300617.
[34] D.K. Wilkins, S.B. Grimshaw, V. Receveur, C.M. Dobson, J.A. Jones, L.J. Smith, Hydrodynamic radii of native and denatured proteins measured by pulse field gradient NMR techniques, Biochemistry 38 (1999) 16424–16431, https://doi.org/10.1021/bi991765q.
[35] L.R. Snyder, J.W. Dolan, High-Performance Gradient Elution: The Practical Application of the Linear-Solvent-Strength Model, Wiley, 2006.
[36] V. Spicer, M. Grigoryan, A. Gotfrid, K.G. Standing, O.V. Krokhin, Predicting retention time shifts associated with variation of the gradient slope in peptide RP-HPLC, Anal. Chem. 82 (2010) 9678–9685, https://doi.org/10.1021/ac102228a.
[37] J. Lenčo, T. Šemlej, M.A. Khalikova, I. Fabrik, F. Švec, Sense and nonsense of elevated column temperature in proteomic bottom-up LC–MS analyses, J. Proteome Res. 20 (2021) 420–432, https://doi.org/10.1021/acs.jproteome.0c00479.
[38] K. Broeckhoven, G. Desmet, Methods to determine the kinetic performance limit of contemporary chromatographic techniques, J. Sep. Sci. 44 (2021) 323–339, https://doi.org/10.1002/jssc.202000779.
[39] K. Broeckhoven, D. Cabooter, F. Lynen, P. Sandra, G. Desmet, The kinetic plot method applied to gradient chromatography: theoretical framework and experimental validation, J. Chromatog. A 1217 (2010) 2787–2795, https://doi.org/10.1016/j.chroma.2010.02.023.
[40] M. Greguš, A.R. Ivanov, S.R. Wilson, Ultralow flow liquid chromatography and related approaches: a focus on recent bioanalytical applications, J. Sep. Sci. 46 (2023) 2300440, https://doi.org/10.1002/jssc.202300440.